Time-resolved protein nanocrystallography using an X-ray free-electron laser

Andrew Aquila,[1,2,*] Mark S. Hunter,[3] R. Bruce Doak,[4] Richard A. Kirian,[4] Petra Fromme,[3] Thomas A. White,[1] Jakob Andreasson,[5] David Arnlund,[6] Saša Bajt,[2] Thomas R. M. Barends,[7,8] Miriam Barthelmess,[2] Michael J. Bogan,[9] Christoph Bostedt,[10] Hervé Bottin,[11] John D. Bozek,[10] Carl Caleman,[1] Nicola Coppola,[12] Jan Davidsson,[5] Daniel P. DePonte,[1] Veit Elser,[13] Sascha W. Epp,[7,14] Benjamin Erk,[7,14] Holger Fleckenstein,[1] Lutz Foucar,[7,8] Matthias Frank,[15] Raimund Fromme,[3] Heinz Graafsma,[2] Ingo Grotjohann,[3] Lars Gumprecht,[1] Janos Hajdu,[5] Christina Y. Hampton,[9] Andreas Hartmann,[16] Robert Hartmann,[16] Stefan Hau-Riege,[15] Günter Hauser,[17] Helmut Hirsemann,[2] Peter Holl,[16] James M. Holton,[18] André Hömke,[7,14] Linda Johansson,[6] Nils Kimmel,[17] Stephan Kassemeyer,[8] Faton Krasniqi,[7,8] Kai-Uwe Kühnel,[14] Mengning Liang,[1] Lukas Lomb,[7,8] Erik Malmerberg,[6] Stefano Marchesini,[18] Andrew V. Martin,[1] Filipe R.N.C. Maia,[5] Marc Messerschmidt,[10] Karol Nass,[19] Christian Reich,[16] Richard Neutze,[6] Daniel Rolles,[7,8] Benedikt Rudek,[7,14] Artem Rudenko,[7,14] Ilme Schlichting,[7,8] Carlo Schmidt,[7,8] Kevin E. Schmidt,[4] Joachim Schulz,[1] M. Marvin Seibert,[5] Robert L. Shoeman,[8] Raymond Sierra,[9] Heike Soltau,[16] Dmitri Starodub,[9] Francesco Stellato,[1] Stephan Stern,[1] Lothar Strüder,[7,17] Nicusor Timneanu,[5] Joachim Ullrich,[7,14] Xiaoyu Wang,[4] Garth J. Williams,[10] Georg Weidenspointner,[20,17] Uwe Weierstall,[4] Cornelia Wunderer,[2] Anton Barty,[1] John C. H. Spence,[4] and Henry N. Chapman[1,19]

[1] *Center for Free-Electron Laser Science, DESY, Notkestraße 85, 22607 Hamburg, Germany*
[2] *Photon Science, DESY, Notkestraße 85, 22607 Hamburg, Germany*
[3] *Department of Chemistry and Biochemistry, Arizona State University, Tempe, Arizona 85287-1604 USA*
[4] *Department of Physics, Arizona State University, Tempe, Arizona 85287 USA*
[5] *Laboratory of Molecular Biophysics, Department of Cell and Molecular Biology, Uppsala University, Husargatan 3 (Box 596), SE-751 24 Uppsala, Sweden*
[6] *Department of Chemistry, Biochemistry, and Biophysics, Göteborg University, SE-405 30 Göteborg, Sweden*
[7] *Max Planck Advanced Study Group, Center for Free Electron Laser Science (CFEL), Notkestraße 85, 22607 Hamburg, Germany*
[8] *Max-Planck-Institut für medizinische Forschung, Jahnstr. 29, 69120 Heidelberg, Germany*
[9] *PULSE Institute and SLAC National Accelerator Laboratory, 2575 Sand Hill Road. Menlo Park, CA 94025, USA*
[10] *LCLS, SLAC National Accelerator Laboratory, 2575 Sand Hill Road. Menlo Park, CA 94025, USA*
[11] *CEA, Institut de Biologie et de Technologies de Saclay, 91191 Gif-sur-Yvette Cedex, France*
[12] *European XFEL GmbH, Albert-Einstein-Ring 19, 22761 Hamburg, Germany*
[13] *Department of Physics, Cornell University, Ithaca, New York 14853 USA*
[14] *Max-Planck-Institut für Kernphysik, Saupfercheckweg 1, 69117 Heidelberg, Germany*
[15] *Lawrence Livermore National Laboratory, 7000 East Avenue, Mail Stop L-211, Livermore, CA 94551, USA*
[16] *PNSensor GmbH, Otto-Hahn-Ring 6, 81739 München, Germany*
[17] *Max-Planck-Institut Halbleiterlabor, Otto-Hahn-Ring 6, 81739 München, Germany*
[18] *Advanced Light Source, Lawrence Berkeley National Laboratory, Berkeley, California 94720, USA*
[19] *University of Hamburg, Luruper Chaussee 149, 22761 Hamburg, Germany*
[20] *Max-Planck-Institut für extraterrestrische Physik, Giessenbachstraße, 85741 Garching, Germany*
[*] *Andrew.Aquila@desy.de*

Abstract: We demonstrate the use of an X-ray free electron laser synchronized with an optical pump laser to obtain X-ray diffraction snapshots from the photoactivated states of large membrane protein complexes in the form of nanocrystals flowing in a liquid jet. Light-induced changes of Photosystem I-Ferredoxin co-crystals were observed at time delays of 5 to 10 μs after excitation. The result correlates with the microsecond kinetics of electron transfer from Photosystem I to ferredoxin. The undocking process that follows the electron transfer leads to large rearrangements in the crystals that will terminally lead to the disintegration of the crystals. We describe the experimental setup and obtain the first time-resolved femtosecond serial X-ray crystallography results from an

#157904 - $15.00 USD Received 11 Nov 2011; revised 16 Dec 2011; accepted 18 Dec 2011; published 23 Jan 2012

irreversible photo-chemical reaction at the Linac Coherent Light Source. This technique opens the door to time-resolved structural studies of reaction dynamics in biological systems.

OCIS codes: (170.7160) Ultrafast technology; (170.7440) X-ray imaging; (140.3450) Laser-induced chemistry; (140.7090) Ultrafast lasers; (170.0170) Medical optics and biotechnology.

References and links

1. F. Schotte, J. Soman, J. S. Olson, M. Wulff, and P. A. Anfinrud, "Picosecond time-resolved X-ray crystallography: probing protein function in real time," J. Struct. Biol. **147**(3), 235–246 (2004).
2. A. B. Wöhri, G. Katona, L. C. Johansson, E. Fritz, E. Malmerberg, M. Andersson, J. Vincent, M. Eklund, M. Cammarata, M. Wulff, J. Davidsson, G. Groenhof, and R. Neutze, "Light-induced structural changes in a photosynthetic reaction center caught by Laue diffraction," Science **328**(5978), 630–633 (2010).
3. T. Graber, S. Anderson, H. Brewer, Y. S. Chen, H. S. Cho, N. Dashdorj, R. W. Henning, I. Kosheleva, G. Macha, M. Meron, R. Pahl, Z. Ren, S. Ruan, F. Schotte, V. Srajer, P. J. Viccaro, F. Westferro, P. Anfinrud, and K. Moffat, "BioCARS: a synchrotron resource for time-resolved X-ray science," J. Synchrotron Radiat. **18**(4), 658–670 (2011).
4. K. Moffat, "The frontiers of time-resolved macromolecular crystallography: movies and chirped X-ray pulses," Faraday Discuss. **122**, 65–77, discussion 79–88 (2003).
5. K. Moffat, D. Szebenyi, and D. Bilderback, "X-ray Laue Diffraction from Protein Crystals," Science **223**(4643), 1423–1425 (1984).
6. F. Schotte, M. Lim, T. A. Jackson, A. V. Smirnov, J. Soman, J. S. Olson, G. N. Phillips, Jr., M. Wulff, and P. A. Anfinrud, "Watching a protein as it functions with 150-ps time-resolved x-ray crystallography," Science **300**(5627), 1944–1947 (2003).
7. D. Bourgeois, B. Vallone, A. Arcovito, G. Sciara, F. Schotte, P. A. Anfinrud, and M. Brunori, "Extended subnanosecond structural dynamics of myoglobin revealed by Laue crystallography," Proc. Natl. Acad. Sci. U.S.A. **103**(13), 4924–4929 (2006).
8. D. Bourgeois, F. Schotte, M. Brunori, and B. Vallone, "Time-resolved methods in biophysics. 6. Time-resolved Laue crystallography as a tool to investigate photo-activated protein dynamics," Photochem. Photobiol. Sci. **6**(10), 1047–1056 (2007).
9. I. Schlichting, S. C. Almo, G. Rapp, K. Wilson, K. Petratos, A. Lentfer, A. Wittinghofer, W. Kabsch, E. F. Pai, G. A. Petsko, and R. S. Goody, "Time-resolved X-ray crystallographic study of the conformational change in Ha-Ras p21 protein on GTP hydrolysis," Nature **345**(6273), 309–315 (1990).
10. M. Cammarata, M. Levantino, F. Schotte, P. A. Anfinrud, F. Ewald, J. Choi, A. Cupane, M. Wulff, and H. Ihee, "Tracking the structural dynamics of proteins in solution using time-resolved wide-angle X-ray scattering," Nat. Methods **5**(10), 881–886 (2008).
11. H. S. Cho, N. Dashdorj, F. Schotte, T. Graber, R. Henning, and P. Anfinrud, "Protein structural dynamics in solution unveiled via 100-ps time-resolved x-ray scattering," Proc. Natl. Acad. Sci. U.S.A. **107**(16), 7281–7286 (2010).
12. S. Westenhoff, E. Nazarenko, E. Malmerberg, J. Davidsson, G. Katona, and R. Neutze, "Time-resolved structural studies of protein reaction dynamics: a smorgasbord of X-ray approaches," Acta Crystallogr. A **66**(2), 207–219 (2010).
13. D. P. DePonte, U. Weierstall, K. Schmidt, J. Warner, D. Starodub, J. Spence, and R. B. Doak, "Gas dynamic virtual nozzle for generation of microscopic droplet streams," J. Phys. D Appl. Phys. **41**(19), 195505 (2008).
14. U. Weierstall, R. B. Doak, and J. C. H. Spence, "A pump-probe XFEL particle injector for hydrated samples," Rev. Sci. Instr. Submitted (2011), *http://arxiv.org/abs/1105.2104*
15. H. N. Chapman, P. Fromme, A. Barty, T. A. White, R. A. Kirian, A. Aquila, M. S. Hunter, J. Schulz, D. P. DePonte, U. Weierstall, R. B. Doak, F. R. N. C. Maia, A. V. Martin, I. Schlichting, L. Lomb, N. Coppola, R. L. Shoeman, S. W. Epp, R. Hartmann, D. Rolles, A. Rudenko, L. Foucar, N. Kimmel, G. Weidenspointner, P. Holl, M. Liang, M. Barthelmess, C. Caleman, S. Boutet, M. J. Bogan, J. Krzywinski, C. Bostedt, S. Bajt, L. Gumprecht, B. Rudek, B. Erk, C. Schmidt, A. Hömke, C. Reich, D. Pietschner, L. Strüder, G. Hauser, H. Gorke, J. Ullrich, S. Herrmann, G. Schaller, F. Schopper, H. Soltau, K. U. Kühnel, M. Messerschmidt, J. D. Bozek, S. P. Hau-Riege, M. Frank, C. Y. Hampton, R. G. Sierra, D. Starodub, G. J. Williams, J. Hajdu, N. Timneanu, M. M. Seibert, J. Andreasson, A. Rocker, O. Jönsson, M. Svenda, S. Stern, K. Nass, R. Andritschke, C. D. Schröter, F. Krasniqi, M. Bott, K. E. Schmidt, X. Wang, I. Grotjohann, J. M. Holton, T. R. M. Barends, R. Neutze, S. Marchesini, R. Fromme, S. Schorb, D. Rupp, M. Adolph, T. Gorkhover, I. Andersson, H. Hirsemann, G. Potdevin, H. Graafsma, B. Nilsson, and J. C. H. Spence, "Femtosecond X-ray protein nanocrystallography," Nature **470**(7332), 73–77 (2011).
16. A. Barty, C. Caleman, A. Aquila, N. Timneanu, L. Lomb, T. A. White, J. Andreasson, D. Arnlund, S. Bajt, T. R. M. Barends, M. Barthelmess, M. J. Bogan, C. Bostedt, J. D. Bozek, R. Coffee, N. Coppola, J. Davidsson, D. P. DePonte, R. B. Doak, T. Ekeberg, V. Elser, S. W. Epp, B. Erk, H. Fleckenstein, L. Foucar, P. Fromme, H. Graafsma, L. Gumprecht, J. Hajdu, C. Y. Hampton, R. Hartmann, A. Hartmann, G. Hauser, H. Hirsemann, P. Holl, M. S. Hunter, L. Johansson, S. Kassemeyer, N. Kimmel, R. A. Kirian, M. Liang, F. R. N. C. Maia, E.

#157904 - $15.00 USD Received 11 Nov 2011; revised 16 Dec 2011; accepted 18 Dec 2011; published 23 Jan 2012

Malmerberg, S. Marchesini, A. V. Martin, K. Nass, R. Neutze, C. Reich, D. Rolles, B. Rudek, A. Rudenko, H. Scott, I. Schlichting, J. Schulz, M. M. Seibert, R. L. Shoeman, R. Sierra, H. Soltau, J. C. H. Spence, F. Stellato, S. Stern, L. Str[UNKNOWN ENTITY &udie;]der, J. Ullrich, X. Wang, G. Weidenspointner, U. Weierstall, C. B. Wunderer, and H. N. Chapman, "Self-terminating diffraction gates femtosecond X-ray nanocrystallography measurements," Nat. Photonics. in press.
17. A. Díaz-Quintana, W. Leibl, H. Bottin, and P. Sétif, "Electron transfer in photosystem I reaction centers follows a linear pathway in which iron-sulfur cluster FB is the immediate electron donor to soluble ferredoxin," Biochemistry **37**(10), 3429–3439 (1998).
18. P. Q. Sétif and H. Bottin, "Laser flash absorption spectroscopy study of ferredoxin reduction by photosystem I: spectral and kinetic evidence for the existence of several photosystem I-ferredoxin complexes," Biochemistry **34**(28), 9059–9070 (1995).
19. P. Sétif, "Ferredoxin and flavodoxin reduction by photosystem I," Biochim. Biophys. Acta **1507**(1-3), 161–179 (2001).
20. V. V. Ptushenko, D. A. Cherepanov, L. I. Krishtalik, and A. Yu. Semenov, "Semi-continuum electrostatic calculations of redox potentials in photosystem I," Photosynth. Res. **97**(1), 55–74 (2008).
21. P. Fromme, H. Bottin, N. Krauss, and P. Sétif, "Crystallization and electron paramagnetic resonance characterization of the complex of photosystem I with its natural electron acceptor ferredoxin," Biophys. J. **83**(4), 1760–1773 (2002).
22. P. Jordan, P. Fromme, H. T. Witt, O. Klukas, W. Saenger, and N. Krauß, "Three-dimensional structure of cyanobacterial photosystem I at 2.5 A resolution," Nature **411**(6840), 909–917 (2001).
23. P. Fromme and H. T. Witt, "Improved isolation and crystallization of Photosystem I for structural analysis," Biochem. Biophys. Acta **1365**(1-2), 175–184 (1998).
24. H. Bottin and B. Lagoutte, "Ferredoxin and flavodoxin from the cyanobacterium Synechocystis sp PCC 6803," Biochim. Biophys. Acta **1101**(1), 48–56 (1992).
25. P. Emma, R. Akre, J. Arthur, R. Bionta, C. Bostedt, J. Bozek, A. Brachmann, P. Bucksbaum, R. Coffee, F.-J. Decker, Y. Ding, D. Dowell, S. Edstrom, A. Fisher, J. Frisch, S. Gilevich, J. Hastings, G. Hays, Ph. Hering, Z. Huang, R. Iverson, H. Loos, M. Messerschmidt, A. Miahnahri, S. Moeller, H.-D. Nuhn, G. Pile, D. Ratner, J. Rzepiela, D. Schultz, T. Smith, P. Stefan, H. Tompkins, J. Turner, J. Welch, W. White, J. Wu, G. Yocky, and J. Galayda, "First lasing and operation of an Ångstrom wavelength free-electron laser," Nat. Photonics **4**(9), 641–647 (2010).
26. J. D. Bozek, "AMO instrumentation for the LCLS X-ray FEL," Eur. Phys. J. Spec. Top. **169**(1), 129–132 (2009).
27. L. Strüder, S. Epp, D. Rolles, R. Hartmann, P. Holl, G. Lutz, H. Soltau, R. Eckart, C. Reich, K. Heinzinger, C. Thamm, A. Rudenko, F. Krasniqi, K. U. Kühnel, C. Bauer, C. D. Schröter, R. Moshammer, S. Techert, D. Miessner, M. Porro, O. Hälker, N. Meidinger, N. Kimmel, R. Andritschke, F. Schopper, G. Weidenspointner, A. Ziegler, D. Pietschner, S. Herrmann, U. Pietsch, A. Walenta, W. Leitenberger, C. Bostedt, T. Möller, D. Rupp, M. Adolph, H. Graafsma, H. Hirsemann, K. Gärtner, R. Richter, L. Foucar, R. L. Shoeman, I. Schlichting, and J. Ullrich, "Large-format, high-speed, X-ray pnCCDs combined with electron and ion imaging spectrometers in a multipurpose chamber for experiments at 4th generation light sources," Nucl. Instrum. Methods Phys. Res. A **614**(3), 483–496 (2010).
28. J. M. Glownia, J. Cryan, J. Andreasson, A. Belkacem, N. Berrah, C. I. Blaga, C. Bostedt, J. Bozek, L. F. DiMauro, L. Fang, J. Frisch, O. Gessner, M. Gühr, J. Hajdu, M. P. Hertlein, M. Hoener, G. Huang, O. Kornilov, J. P. Marangos, A. M. March, B. K. McFarland, H. Merdji, V. S. Petrovic, C. Raman, D. Ray, D. A. Reis, M. Trigo, J. L. White, W. White, R. Wilcox, L. Young, R. N. Coffee, and P. H. Bucksbaum, "Time-resolved pump-probe experiments at the LCLS," Opt. Express **18**(17), 17620–17630 (2010).
29. T. A. White, R. A. Kirian, A. V. Martin, A. Aquila, K. Nass, A. Barty, and H. N. Chapman, "CrystFEL: A software suite for snapshot serial crystallography," J. Appl. Cryst. in press.
30. R. A. Kirian, T. A. White, J. M. Holton, H. N. Chapman, P. Fromme, A. Barty, L. Lomb, A. Aquila, F. R. N. C. Maia, A. V. Martin, R. Fromme, X. Wang, M. S. Hunter, K. E. Schmidt, and J. C. Spence, "Structure-factor analysis of femtosecond microdiffraction patterns from protein nanocrystals," Acta Crystallogr. A **67**(2), 131–140 (2011).

1. Introduction

A full understanding of the function and interactions of biological macromolecules requires a determination of their three-dimensional (3D) atomic structures and the dynamics of the rearrangement of these structures as reactions occur. Time-resolved Laue Crystallography has been developed to determine changes in the electron densities of molecules, which can be related to the trajectories of atoms in proteins over timescales from picoseconds to seconds [1–6]. In the Laue method, diffraction patterns are recorded from a single crystal in a selected set of angular orientations using broad bandwidth X-ray pulses. Time-resolved measurements require a fast trigger for initiating the reaction in the crystal, which is then probed at different time points along the reaction coordinate, with the crystal in different orientations, until complete data sets are obtained. Both reversible (e.g., [7,8]) and irreversible (e.g., [9])

#157904 - $15.00 USD Received 11 Nov 2011; revised 16 Dec 2011; accepted 18 Dec 2011; published 23 Jan 2012

reactions have been studied. The latter are complicated by the fact that for short-lived intermediates or reactions resulting in destruction of the crystal lattice, fresh crystals need to be used for each time-point and orientation, which can make the experiments impractical. Therefore, ultra-fast Laue methods are usually carried out on reversible photo-reactions and has been very successfully applied to protein crystals with small unit cells, for which large, highly ordered and radiation resistant single protein crystals could be grown. The analysis of conformational changes in large protein complexes by time-resolved Laue crystallography is, however, hampered by the inherent problem of overlapping reflections, and is normally used only to study reproducible processes that can be repeatedly excited by an external trigger.

A complementary approach for studying protein dynamics with structural sensitivity is wide-angle X-ray scattering (WAXS) [10–12], where data are collected from proteins in a solution that flows across the pulsed X-ray source. Irreversible reactions can be studied since the sample is constantly refreshed. However, the orientationally averaged scattering pattern gives less structural information than achievable by crystallography.

We describe here a new approach that combines elements of time-resolved crystallography and WAXS, in which diffraction patterns from diffracting microcrystals flowing in liquid suspension [13, 14] are recorded using femtosecond pulses from an X-ray free-electron laser (FEL). Each 70 fs X-ray pulse generates a diffraction pattern and then terminates before the subsequent photoelectron cascade destroys the microcrystal [15]. Since the sample is replenished after every shot, irreversible conformational changes of crystals can be studied. The advent of X-ray FELs has enabled new approaches to molecular structure determination, using crystals that are too small or too radiation sensitive for analysis at conventional synchrotron facilities [15]. The coherent combination of scattered intensities to form Bragg peaks provides much higher resolution data than can be achieved by WAXS. Individual microcrystal diffraction patterns can either be assembled into time-resolved "virtual" powder diffraction patterns [16] or, after indexing, combined into a time-resolved three-dimensional set of structure factors.

In this experiment we induced structural changes in Photosystem I-Ferredoxin co-crystals (PSI-fd) using an optical laser. Photosystem I (PSI) occurs in all green plants, and is responsible for producing the chemical energy, by driving the reduction from NADP + to NADPH, needed to transform carbon dioxide into sugar. Light excitation of PSI leads to charge separation in which its primary donor chlorophyll, P700, is excited and an electron transferred by a chain of electron carriers across the membrane over a distance of 60 Å to the terminal electron acceptor in PSI the iron-sulfur cluster. After ferredoxin, the soluble electron transfer protein, docks to the acceptor site of PSI it is reduced. The electron transfer is multi-phasic with time constants of 500 ns and 2 μs [17–20] as determined by time-resolved optical spectroscopy and is followed by undocking of reduced ferredoxin from PSI. Ferredoxin leaves its binding site to convey the electron to FNR (ferredoxin-NADP + reductase), which finally reduces NADP + to NADPH. This electron transfer reaction is one of the key steps in oxygenic photosynthesis, understanding the dynamics of the transfer and subsequent undocking of the ferredoxin can help us determine how this molecular machine operates. It has been shown previously by EPR spectroscopy that the PSI-fd co-crystals contain a photoactive complex of PSI with ferredoxin [21] and crystals dissolve in less than a second upon excitation with visible light at room temperature.

PSI-fd was chosen as a test case because of the irreversible nature of the conformational changes in the crystal and the fast rate of dissolution that occurs as a consequence of those changes. This fast dissolution of the crystals prevents measurements of photoexcited crystals to be carried out at conventional synchrotron sources. A schematic of our serial time-resolved nanocrystallography experiment is shown in Fig. 1, and is similar to previous femtosecond nanocrystallography experiments [15]. The main modification required to carry out time-resolved diffraction is the addition of the pulsed optical laser that illuminates the liquid jet in and near the interaction region. In the future, other reaction triggers, such as the mixing of

#157904 - $15.00 USD Received 11 Nov 2011; revised 16 Dec 2011; accepted 18 Dec 2011; published 23 Jan 2012

substrate to a suspension of crystals that perform enzymatic reactions, can be implemented enabling the extension of this method to the determination of protein dynamics in systems that are not triggered by light.

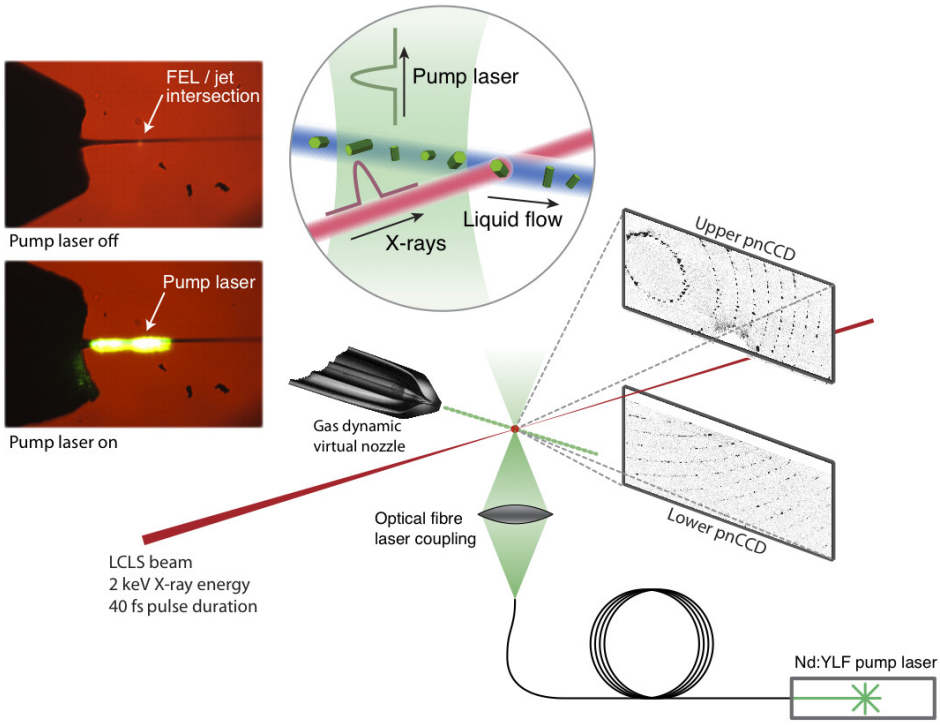

Fig. 1. Experimental setup and intersection of the 3 interacting beams: X-rays, pump laser, and the liquid jet containing the co-crystals. The upper left insert shows the thermal glow of the 2 keV X-rays interacting with the liquid jet. The lower insert shows the scatter from the frequency-doubled Nd:YAG pump laser from the liquid jet. The overlap of the two beams (liquid jet and X-rays) can be seen, with the pump laser intersecting the liquid jet of co-crystals and extending upstream towards the nozzle. The pump laser is extended upstream of the X-ray pulse to compensate for the approximately 130 µm travel of the crystals between the pump and probe pulses for the 10 µs delay time.

2. Experimental description

2.1 Crystal preparation

Photosystem I is a large membrane protein complex. It is a trimer with a molecular mass of 1,058,000 Da, consisting of 36 proteins and 381 cofactors [22] that catalyzes the second step in the conversion of sunlight into chemical energy. The crystals contain one PSI trimer and 3 ferredoxin molecules in the asymmetric unit, which therefore contains 39 protein subunits and 384 cofactors. Co-crystals of PSI with ferredoxin of 500 nm to 2 µm size were grown by a modification of the method described in [21] for growth of large single crystals. PSI was isolated from the thermophilic cyanobacterium *T. elongatus* as described in [23], and ferredoxin was isolated as described in [24]. Nanocrystals were grown overnight at SLAC in complete darkness at 20°C using the batch method with 35 µM of the primary donor P700, which is directly related to the number of PSI electron transfer chains, and 38.5 µM ferredoxin in the presence of 25% polyethylene glycol (PEG 400). The buffer solution contained 100 mM HEPES at pH 7.5, 150 mM $CaCl_2$, and 0.02% of the detergent beta-dodecylmaltoside.

#157904 - $15.00 USD Received 11 Nov 2011; revised 16 Dec 2011; accepted 18 Dec 2011; published 23 Jan 2012

2.2 LCLS endstation

Our time-resolved femtosecond X-ray nanocrystallography experiments were carried out at the Linac Coherent Light Source (LCLS) [25] at SLAC in the CFEL-ASG Multi Purpose (CAMP) instrument on the Atomic, Molecular, and Optical Science beamline [26]. A suspension of the crystals at room temperature in their mother liquor was injected in vacuum into the path of the focused X-ray beam. The gas-focused liquid jet had a diameter of about 4 μm, matched to the X-ray focal area of 7 μm^2. The X-ray pulse repetition rate was 60 Hz and X-ray scattering patterns were read out on a set of pnCCD detectors [27] after each pulse. If a crystal was in the path of the X-ray pulse when it arrived at the jet, a diffraction pattern was recorded. These crystal "hits" were sorted from the data set after the experiment. The X-ray photon energy was 2 keV (0.69 nm wavelength) and the electron bunch, used to generate the X-ray pulses, had a duration of 70 fs. (We emphasize that the much briefer femtosecond X-ray pulses are used to avoid radiation damage effects, and were not chosen to determine the time-resolution of the experiment). The detector, covering a maximum scattering angle of 45.6°, recorded patterns with a maximum resolution of 0.8 nm. With an estimated beamline transmission of 20%, FEL pulses with typical energies around 3 mJ gave an irradiance greater than 10^{17} W/cm^2/pulse in the focus, and so the single-pulse dose to the PSI-fd crystals was about 3 GGy.

2.3 Sample delivery and visible pump laser

The injector system supplied a continuous stream of hydrated bioparticles to the pump laser and X-ray beam in vacuum, and was constructed as an integrated unit encapsulated in a shroud tube (see [14] for full details of the pump-probe hydrated particle injector). The long 25.4 mm diameter tube contained the gas-focused liquid jet, with a 2 mm diameter hole for the X-ray beam entrance and a conical exit hole that allowed high-angle scattering to be detected in the far field. The shroud was pumped by a turbomolecular pump, which helped to maintain a low pressure in the main chamber and reduced air scatter. For the time-resolved measurements, the pump laser was introduced into the system through an optical fiber, the output of which was focused onto the jet. A 532 nm wavelength laser (frequency-doubled Nd:YAG) was used to excite the PSI-fd co-crystals. The 8 μJ, approximately 10 ns pump pulses, focused to a 380 μm diameter area, provided a factor of 10 times more fluence than the minimum required to excite every PSI complex in a crystal of 2 μm diameter. The pulses were synchronized with LCLS pulses [28]. The experiment required the spatial overlap of three perpendicular beams: the 7 μm^2 focused X-ray FEL pulses, the 4 μm diameter liquid jet containing PSI-fd co-crystals, and the visible pump laser covering a 380 μm diameter region as seen in Fig. 1. The alignment process was greatly facilitated by using a CCD-based in situ in-vacuum microscope built into the shroud. This microscope provided real-time images of the interaction region with 2 μm spatial resolution. The scattering of the visible pump laser from the jet could be seen on the microscope display. With the pump laser off, the interaction of the FEL beam with the liquid jet was visualized on the display by the afterglow of the plasma formed by the X-ray pulse. Temporal overlap was achieved using the LCLS timing system to a precision of better than a picosecond, easily sufficient for the microsecond time delays required.

For the relatively long microsecond delays between pump and probe of these experiments, it was necessary to consider the velocity of the flowing suspension and the distance a crystal travels after exposure by the pump laser. It is important to ensure that any crystal hit by an X-ray pulse fell within the illumination area of the pump at an earlier time interval equal to the pump laser delay, and hence was excited prior to being probed. The jet velocity, the diameter of the pump laser focus on the jet and the longest distance beyond the nozzle exit where the X-ray beam intersected the jet thus limit the maximum delay achievable. We also aimed to avoid the 'breakup region' of the jet, where the continuous liquid column broke up into a

#157904 - $15.00 USD Received 11 Nov 2011; revised 16 Dec 2011; accepted 18 Dec 2011; published 23 Jan 2012

stream of droplets, which typically formed about 200 µm from the nozzle. The droplets downstream from the breakup region were about twice the diameter of the liquid column, which resulted in higher background scattering from the solution. With a typical flow rate of about 10 µl/minute, the velocity of the 4 µm diameter jet was 13 m/s. The pump pulse illuminated the entire jet length from the nozzle to the X-ray interaction, allowing measurements from zero delay up to a maximum delay of 15 µs. We made measurements up to a delay of 10 µs to account for uncertainty in jet velocity.

2.4 Data collection

Data frames were recorded continuously at a rate of 60 Hz or 216,000 frames per hour. We collected data sets with three different time delays: two positive time delays of 5 µs and 10 µs, and a ground state data set with the pump laser triggered 10 µs after the LCLS FEL pulse. This negative time delay was taken as the ground state data set to ensure statistically identical background signals between the data sets, since the pnCCD detectors were sensitive to the visible light of the pump laser. Data collection was performed cycling between the three delay times, switching every 15 minutes to ensure that any changes in signal were caused by the pump laser and to reduce systematic errors.

3. Results and discussion

Each pnCCD frame was first corrected for variations in gain and background, and then a time-windowed average background was subtracted from each frame on a pixel by pixel basis to further reduce noise. Each data frame was then searched for Bragg peaks using a threshold and morphological analysis algorithm, producing a list of peak locations and intensities. Any frame with fewer than three peaks was rejected, as was any peak detected in the region of the detector known to contain scattering from the liquid jet or any region affected by electronic artifacts. About 780,000 frames of data were collected in total for all time delays (the ground state plus two positive time delays). Of those, approximately 7% (59,154) of the frames showed diffraction patterns containing three or more Bragg peaks. A summary of the data is shown in Table 1.

Table 1. Statistical summary of the data collected for the various time delays.

	Ground State	5 µs excited state	10 µs excited state
Frames Collected	396780	219960	162420
% w/ 3+ peaks	7.23%	8.84%	6.77%
% w/ 10+ peaks	2.29%	3.11%	2.03%
% indexed (# indexed/ # 10+ peaks)	17.98%	15.96%	9.60%

#157904 - $15.00 USD Received 11 Nov 2011; revised 16 Dec 2011; accepted 18 Dec 2011; published 23 Jan 2012

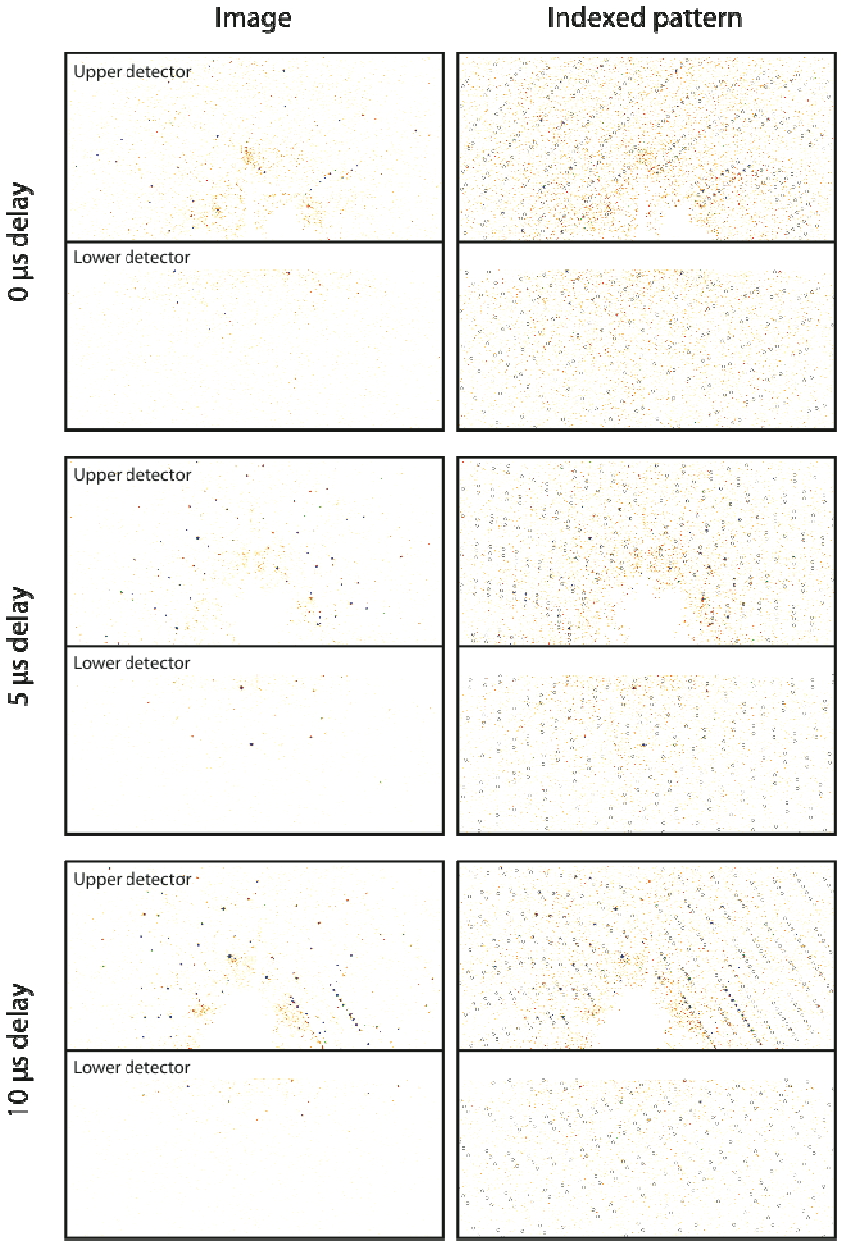

Fig. 2. Single-shot, single crystal diffraction patterns, from the pnCCD detectors, of PSI-fd (top) in the dark state, (middle) in the 5 µs pumped state, and (bottom) the 10 µs pumped state. The images on the right side are the same as the corresponding left side image, except predicted peak locations from indexing are shown in gray circles. Partial reflections were observed containing between 10 to 500 photons per peak with a background level of around 2 photons caused by water scatter, fluorescence, and detector noise.

Representative single crystal diffraction patterns from each time delay are shown in Fig. 2. While many of the single-shot crystal diffraction patterns could be indexed successfully [29], as shown in Table 1, we did not collect the estimated 40,000 indexable diffraction patterns for each time delay required to extract structure factors by performing a Monte Carlo angular

#157904 - $15.00 USD Received 11 Nov 2011; revised 16 Dec 2011; accepted 18 Dec 2011; published 23 Jan 2012

integration across each rocking curve [30], which would have enabled the calculation of electron density maps. Instead, we evaluated the data by assembling "virtual powder diffraction patterns". In this method, the total scattered intensity from all crystals with 3 or more peaks is plotted as a function of scattering angle (momentum transfer) $|K| = 1/d = 2 \sin \theta / \lambda$, where 2θ is the scattering angle, λ the X-ray wavelength and d is the crystallographic "d-spacing" spatial frequency. The partial reflection intensity was determined for each Bragg peak. This was performed on a frame-by-frame basis using individually measured value of λ for each frame, in order to account for the shot-to-shot wavelength variation inherent to the self-amplified stimulated emission (SASE) process of the LCLS. Summing intensities at each momentum transfer produced "virtual" powder diffraction patterns at each time delay (as opposed to conventional powder diffraction where data are collected in parallel, each crystal is exposed to X-rays one by one). We note that summation of individual crystal diffraction patterns enables better removal of systematic background than conventional powder diffraction methods.

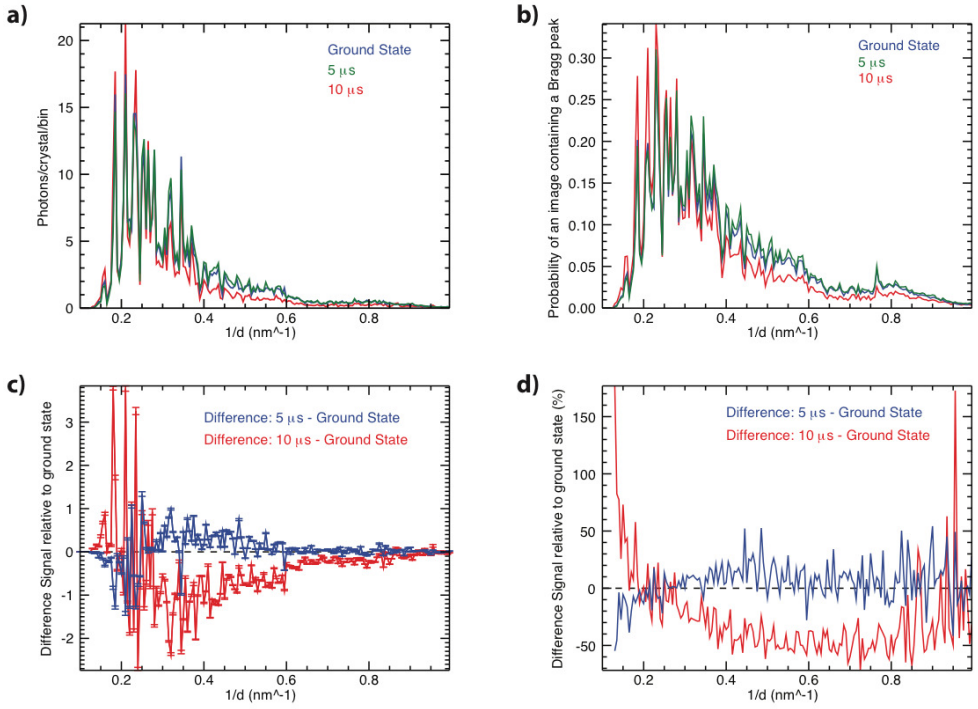

Fig. 3. (a) The 1D virtual powder patterns for the ground state and two positive time delays for PSI-fd co-crystals. The intensities were linearly scaled to minimize the signal difference between for the different excited delays to the ground state. The powder patterns show the average number of photons scattered per crystal hit with in a histogram bin size of q = 0.005 nm^{-1}. The area under the curve corresponds to 393.3, 406.6, and 378.1 average diffracted photons per crystal detected for the dark, 5 μs, and 10 μs data sets respectively. (b) Counting statistics of the number of peaks used in the virtual powder pattern recorded as a function of 1/d. The area under the curve corresponds to the average number of peaks per crystal diffraction pattern of 10.8, 11.5, and 9.9 peaks/pattern for the dark, 5 μs, and 10 μs data sets respectively. (c) Relative difference signal between the ground state and the excited states as a function of resolution. Error bars on the data points are 3σ errors. (d) Difference signal expressed as a percentage change.

Figure 3a shows the virtual powder plots for the different time delays. The data sets varied in crystal orientation, crystal size and number of collected frames, so scaling between data sets was required. The powder plots were linearly scaled to minimize the root mean square

#157904 - $15.00 USD Received 11 Nov 2011; revised 16 Dec 2011; accepted 18 Dec 2011; published 23 Jan 2012

differences between the three powder plots. The 3σ errors, shown in Fig. 3c, were calculated from the distribution of the partial reflection intensity in each histogram bin q_i by:

$$\sigma_T(q_i) = N\left\{\frac{\sigma_d(q_i)}{\sqrt{N}}\right\}$$

where σ_T is the 1σ error of the total and σ_d is the 1σ error of the distribution of partial reflections located in the q_i histogram bin, and N is the number of partial reflections in the given bin. The value in the {} is the standard error of the mean intensity. To obtain the standard error of the total, we use the fact that $I_{total} = N * I_{mean}$.

The changes in the virtual powder diffraction patterns between the dark images (blue in Figs. 3a and 3b), the 5μs time delay (green) and the 10 μs time delay (red) show different trends. The 5 μs data set shows a slight, 1σ, increase of the intensity over most of the measured K range whereas the 10 μs data set shows a significant, 5 to 6σ, decrease over the same range. The decrease in the 10 μs data set could be explained by the irreversible nature of the reactions that occur after the electron has been transferred to ferredoxin, leading to disintegration of the crystals after undocking of ferredoxin from PSI. While the decrease in signal at 10 μs was expected, the slight increase at 5 μs is an unexpected trend that has not been seen before in time resolved studies of reversible reactions by WAXS and Laue crystallography. In particular, we speculate that the data can be described by two processes: a correlated structural change induced by electron transfer in the PSI-fd complex in the 5 μs delay, followed by a disordering of the crystalline lattice that leads to a drop in Bragg intensity as the crystals dissolve. In a dissolving crystal, the decay of Bragg peaks starts at high K, which is seen in the 10 μs data set. Further evidence supporting the hypothesis of the undocking and the dissolution of crystals are changes in the average number of Bragg peaks as a function of resolution for the three time delays (Fig. 3b), which shows a strong decrease of the number of high K Bragg peaks in the 10 μs data set. Since the X-ray pulse duration, wavelength and fluence were held constant for all measurements, to within the jitter of the SASE process, it is unlikely that the observed changes arise from differences in the X-ray dose and subsequent vaporization of the sample — such X-ray induced changes would be identical regardless of time delay. These results are in the time range of the kinetics reported for the electron transfer between PSI and ferredoxin [22,23], supporting the interpretation of the differences in the virtual powder patterns as arising from light-induced conformational changes in the protein crystals.

4. Conclusion

We have developed a new method for time-resolved pump/probe study of the dynamics of hydrated single nano- to micron-sized crystals using femtosecond X-ray diffraction measurements on an irreversible reaction, and demonstrated this technique on a large complex membrane protein involved in solar energy conversion. The method allows excitation and detection of conformational changes by collection of many snapshots of single crystals with time delays between picoseconds and tens of microseconds, or possibly longer using a slower jet. The results reveal significant changes to the nanocrystal samples after excitation by visible light in Photosystem I, using excitation with visible light at delays of 5 and 10 μs between the visible light trigger and the collection of the diffraction patterns by the femtosecond FEL X-ray pulse. This time range matches the kinetics previously reported for electron transfer between PSI and ferredoxin. This initial study paves a clear path towards the further development of time-resolved nanocrystallography, with the ultimate goal of producing molecular movies of biomolecules at work.

#157904 - $15.00 USD Received 11 Nov 2011; revised 16 Dec 2011; accepted 18 Dec 2011; published 23 Jan 2012

Acknowledgments

Experiments were carried out at the Linac Coherent Light Source national user facilities operated by Stanford University on behalf of the U.S. Department of Energy (DOE), Office of Basic Energy Sciences. We acknowledge support from the Helmholtz Association; the Max Planck Society for funding the development and operation of the CAMP instrument within the ASG at CFEL; DOE through the PULSE Institute at the SLAC National Accelerator Laboratory, and by the Lawrence Livermore National Laboratory under Contract DE-AC52-07NA27344; the US National Science Foundation (awards 0417142 and MCB-1021557); the US National Institutes of Health (award 1R01GM095583-01 ROADMAP); the Joachim Herz Stiftung, the Swedish Research Council (VR), and STINT . We thank the staff of the LCLS for their support in carrying out these experiments.

#157904 - $15.00 USD Received 11 Nov 2011; revised 16 Dec 2011; accepted 18 Dec 2011; published 23 Jan 2012

Author/s:

Aquila, A; Hunter, MS; Doak, RB; Kirian, RA; Fromme, P; White, TA; Andreasson, J; Arnlund, D; Bajt, S; Barends, TRM; Barthelmess, M; Bogan, MJ; Bostedt, C; Bottin, H; Bozek, JD; Caleman, C; Coppola, N; Davidsson, J; DePonte, DP; Elser, V; Epp, SW; Erk, B; Fleckenstein, H; Foucar, L; Frank, M; Fromme, R; Graafsma, H; Grotjohann, I; Gumprecht, L; Hajdu, J; Hampton, CY; Hartmann, A; Hartmann, R; Hauriege, S; Hauser, G; Hirsemann, H; Holl, P; Holton, JM; Hoemke, A; Johansson, L; Kimmel, N; Kassemeyer, S; Krasniqi, F; Kuehnel, K; Liang, M; Lomb, L; Malmerberg, E; Marchesini, S; Martin, AV; Maia, FRNC; Messerschmidt, M; Nass, K; Reich, C; Neutze, R; Rolles, D; Rudek, B; Rudenko, A; Schlichting, I; Schmidt, C; Schmidt, KE; Schulz, J; Seibert, MM; Shoeman, RL; Sierra, R; Soltau, H; Starodub, D; Stellato, F; Stern, S; Strueder, L; Timneanu, N; Ullrich, J; Wang, X; Williams, GJ; Weidenspointner, G; Weierstall, U; Wunderer, C; Barty, A; Spence, JCH; Chapman, HN

Title:

Time-resolved protein nanocrystallography using an X-ray free-electron laser

Date:

2012-01-30

Citation:

Aquila, A., Hunter, M. S., Doak, R. B., Kirian, R. A., Fromme, P., White, T. A., Andreasson, J., Arnlund, D., Bajt, S., Barends, T. R. M., Barthelmess, M., Bogan, M. J., Bostedt, C., Bottin, H., Bozek, J. D., Caleman, C., Coppola, N., Davidsson, J., DePonte, D. P. ,... Chapman, H. N. (2012). Time-resolved protein nanocrystallography using an X-ray free-electron laser. OPTICS EXPRESS, 20 (3), pp.2706-2716. https://doi.org/10.1364/OE.20.002706.